Computation of the Release Force in a Gear Shrink-Fitted over a Solid Shaft

Omar Bataineh and Ali Al-Hawari
Jordan University of Science and Technology, Irbid, Jordan
Email: omarmdb@just.edu.jo, ahhawari16@eng.just.edu.jo

Abstract— **Estimating the force required to release a gear shrink-fitted over a solid shaft is important for design considerations. In this study, the release force was computed analytically and using the finite element method (FEM). The results were then compared and validated through experiments according to the design of experiments (DOE) technique. Analysis of variance (ANOVA) was used to identify the relevant sources of variability in the experimental results. Two factors were studied in experiments: average surface roughness of the shaft and pulling speed of the universal testing machine. The results showed that the relative error between the analytical and FEM results was 5.4%, which was interpreted by two reasons. First, the analytical results were based on a two-dimensional model, whereas the numerical results were based on a three-dimensional model. Second, the analytical approach used a hollow cylindrical hub geometry to represent the gear, whereas the FEM model used a more realistic virtual gear geometry. The ANOVA results showed that surface roughness has a significant effect on the experimental results of the release force, but the pulling speed was not an influential factor. The analytical and FEM values of the release force were found to be within the confidence interval established about the mean release force obtained from experiments.**

Index Terms— **shrink-fit assembly, shaft-gear connection, finite element method, DOE, ANOVA**

NOMENCLATURE

δ	Interference between the hub and shaft (mm)
R_f	Actual radius of contact between the hub and shaft (mm)
R_S	Outside radius of the shaft (mm)
R_{Ho}	Outside radius of the hub (mm)
R_{Hi}	Inside radius of the hub (mm)
δ_{rH}	Radial displacement of the hub (mm)
δ_{rS}	Radial displacement of the shaft (mm)
E_S	Modulus of elasticity for the shaft material (MPa)
E_H	Modulus of elasticity for the hub material (MPa)
v_S	Poisson's ratio for the shaft material
v_H	Poisson's ratio for the hub material

I. INTRODUCTION

Interference fits are one type of mechanical fits where an oversized component, such as a shaft, is forced into a hub that has a slightly smaller internal diameter. When fitted over the shaft, some deformation occurs to the hub by increasing its inside diameter, and to the shaft by decreasing its outside diameter [1]. The interference-fit joint has many advantages such as high rigidity, high fatigue life, and high load-bearing compared to other connection types (e.g. key and pin connections). Such characteristics of interference-fit joints make them suitable for use in various applications including aerospace, energy, transportation, and agriculture [2]. Interference fits are widely used with gears in all types of machinery [3].

The interference fit itself is divided, according to the amount of interference and the load type, into three classes: Press, Medium Drive, and Shrink fit. The designated symbols for the standard press, medium drive, and shrink fits according to the International Organization for Standardization (ISO) are (H7/p6), (H7/s6), and (H7/u6), respectively [4]. Generally, the rigidity and strength of assemblies depend on various parameters such as the amount of interference, material properties, physical dimensions, and friction coefficient of contact surfaces [5]. In the shrink-fit type, a temperature change is necessary to produce a thermal expansion in the hub in order to slip it over the shaft, after which it cools and contracts. This type of fit is suitable when the temperature gradient is not high enough to cause significant changes in the microstructure of the assembly materials, thus degrading their mechanical properties. In the last type, the medium drive fit uses both force and thermal expansion to assemble the hub over the shaft.

Predicting the release force required to break the shaft/hub joint is important for design considerations. Analytical models can be relied on to provide approximate solutions in many cases. However, in cases where complex geometries are encountered, numerical methods such as the Finite Element Method (FEM) or Finite Element Analysis (FEA) give better results and more accurate estimates [6]. These numerical methods are used in many engineering filed such as material engineering [7], [8], mechanical design [9], [10], manufacturing technology [11], and many more examples.

Laghzale and Bouzid [12] developed an analytical model to study the residual stresses and deformations in the elasto-plastic region of joints assembled by an

interference fit. The finite element method (FEM) was used to validate the results, and the results were very well. Murčinková et al. [13] studied the press-fitted joints and their dimensional parameters using an analytical and numerical method. Yamamoto and Ishiduka [14] evaluated the effect of interference fit on the stress concentration of the transition wheel fitted over an axle shaft using analytical, numerical, and experimental evaluation. Zhang et al. [15] introduced a study of the fretting wear and fatigue in the press-fitted shaft using finite element modeling. Song et al. [16] presented a study of the effective diameter of the hub shrink-fitted over a shaft using Lame's equations and finite element analysis. Chu et al. [17] studied the effect of the press and shrink fit on the torque capacity of shaft/gear connection using analytical, numerical, and experimental analysis. Mascle et al. [18] studied the effects of the surface roughness of the shrink-fitted mating parts and the interference between them on the torque capacity. Raj et al. [19] studied the effects of the roughness, roundness, and cylindricity on the axial-extraction load of a bearing interference-fitted over a shaft. Seifi et al. [20] proposed a method to calculate the coefficient of friction of the contact surface of the interference-fitted joint and studied the effect of the surface roughness on the extraction strength and the wear of the contact surface.

This study is motivated by the fact that none of the relevant studies available in the literature has addressed the variability in the experimental results using the DOE and ANOVA methods. Therefore, the release force in a gear shrink-fitted over a solid shaft will be evaluated using an analytical model, a numerical model, and DOE-based factorial experiments. The analysis of variance will be used to identify the relevant sources of variability in the experimental results. Finally, a comparison will be made between the analytical solution, numerical solution, and experimental results.

II. ANALYTICAL MODEL

Consider the interference fit between a hub and a hollow shaft as shown in Fig. 1. The main methodology for deriving the analytical model to estimate the release force in a gear shrink-fitted over a solid shaft is given by [21]. An approximate closed-form analytical solution for the contact pressure for a hub fitted over a solid shaft is given by:

$$P = \frac{R_S - R_{H_i}}{\frac{R_f}{E_H}\left(\frac{R_{H_o}^2 + R_f^2}{R_{H_o}^2 - R_f^2} + \nu_H\right) + \frac{R_f}{E_s}(1 - \nu_s)} \quad (1)$$

Where the actual radius of contact between the hub and shaft is given by:

$$R_f = R_s + \frac{E_H(R_s - R_{H_i})(\nu_s - 1)}{E_s\left(\frac{R_{H_o}^2 + R_s^2}{R_{H_o}^2 - R_s^2} + \nu_H\right) - E_H(\nu_s - 1)} \quad (2)$$

In the experiment, the assembly or disassembly of an interference fit requires applying a release force FR to overcome the friction force that results from the contact pressure between the hub and the shaft. This release force can be estimated as:

$$F_R = \mu_s P (2\pi R_f L) \quad (3)$$

If the shaft and hub are made from the same material or the shaft and hub materials have the same mechanical properties. In other words, $E_s = E_H = E$ and $\nu_s = \nu_H = \nu$, then Eq. (1) and Eq. (2) become:

$$P = \frac{\delta E \left(R_{H_o}^2 - R_f^2\right)}{2 R_f R_{H_o}^2} \quad (4)$$

$$R_f = R_s + \frac{\delta\left(R_{H_o}^2 - R_s^2\right)(\nu - 1)}{2R_{H_o}^2} \quad (5)$$

Where the radial interference (δ) between the hub and shaft is equal to $R_s - R_{H_i}$
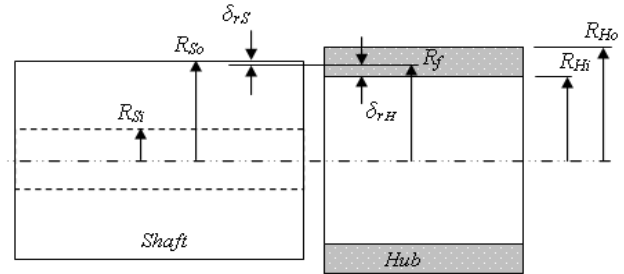
Figure 1. Dimensions of a hollow shaft and a hub interference fit prior to assembling.

III. NUMERICAL MODEL

A three-dimensional finite element model was used to predict the release force in the gear shrink-fitted over the solid shaft, as shown in Fig. 2. This model was realized with the COMSOL Multiphysics FEA software. The type of finite element mesh which was used for this model is a tetrahedron because this type is suitable for complex geometries and gives better and more accurate results.
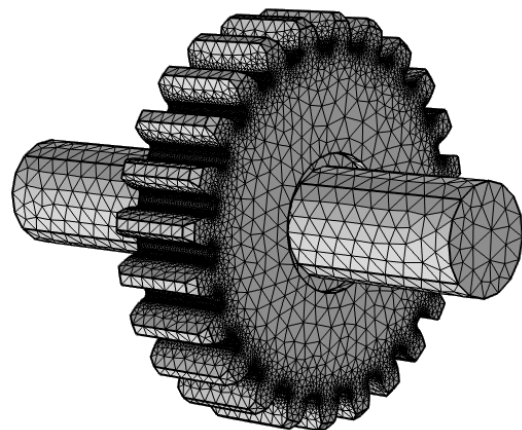
Figure 2. Three-dimensional FEM model.

The internal and external diameters and width of the gear are 28, 86, and 26 mm, respectively. The shaft has a 28.05 mm diameter and 150 mm length, as shown in Fig. 3. Based on these geometries, the radial interference (δ) is $14.025 - 14 = 0.025$ mm and the contact length (L) is $26 - 3 = 23$ mm. The static coefficient of friction (μ_s) that was used in this study is 0.12 and this value was obtained experimentally.
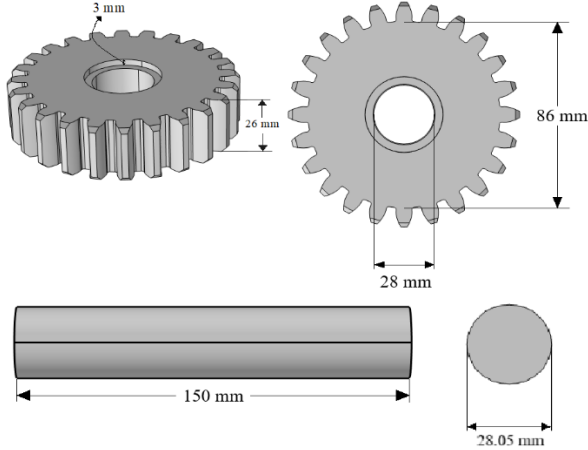
Figure 3. Geometric dimensions of the gear and shaft.

A. Material Properties

An AISI 1020 low-carbon steel was used for the shaft material, and an AISI 6150 alloy steel, which additionally includes chromium and vanadium, was used for the gear material. The detailed chemical composition (wt.%) of the shaft and gear materials is presented in Table I. The mechanical properties (elastic properties) of the shaft and gear materials are listed in Table Ⅱ.

TABLE I.   TYPE SIZES FOR CAMERA-READY PAPERS

Material	C	Mn	Si	P	S	Cr	V
AISI 6150 alloy steel	0.48-0.53	0.70-0.90	0.15-0.30	$\leq$ 0.035	$\leq$ 0.04	0.80-1.10	$\geq$ 0.15
AISI 1020 steel	0.17-0.23	0.30-0.60	0.15-0.30	$\leq$ 0.04	$\leq$ 0.05		

TABLE II.   ELASTIC PROPERTIES OF AISI 1020 AND AISI 6150 ALLOY STEEL

Material	Modulus of elasticity (GPa)	Poisson's ratio	Yield strength (MPa)
AISI 6150 alloy steel	200	0.29	415
AISI 1020 steel	200	0.29	295

B. Boundary Conditions

The physics interface used in this study is the solid mechanics because it is used for general structural analysis of 2D, 3D, or axisymmetric bodies. The solid mechanics interface is based on solving Navier's equations, and results such as displacements, stresses, and strains are computed. Also, the stationary study was used because the field variables do not change over time.

IV.   EXPERIMENTAL WORK

A DOE-based factorial experiments and ANOVA were used to identify the relevant sources of variability in the experimental results and interpret the difference and error between the analytical, numerical, and experimental results. The potential sources of variability in the experimental measurements that were studied are the average surface roughness of the shaft - R_a (μm) and the pulling speed (mm/min) of the universal testing machine, as these factors are not defined in the analytical and numerical models. Thus, a two-factor factorial experiments with two replicates was conducted to study the effect of R_a, pulling speed, and the interaction between them on the release force. R_a that was studied has two levels (Smooth and Rough) and the testing speed that was studied has two levels (2 and 4 mm/min). Based on this design, there are 8 combinations of the two-factor levels that need to be run randomly. This randomization is very important to eliminate the effect of nuisance factors [22]–[26] such as roughness heterogeneity for all surface points.

A. Specimen Preparation

Eight shafts were made with two nominal values of R_a as smooth and rough. Four shafts have a smooth surface and the other four have a rough surface. The variance between the levels (smooth and rough) was made by special conditions on the turning process for every four shafts such as using a specific fine and coarse sandpaper and changing the spindle speed of the turning process from low to high. Each of the four shafts was made with the same conditions of turning and smoothing processes in order to obtain the same specimens and avoid the effect of nuisance factors. The application of these conditions contributed to achieving a clear difference between the roughness values as shown in Table Ⅲ. This table shows the roughness measurement that was taken in eight lines on the contact surface of the smooth and rough shafts. Fig. 4 shows the smooth and rough shafts that were used for the experiments in this study.

Figure 4. Rough and smooth shafts.

TABLE III. ROUGHNESS MEASUREMENT THAT WAS TAKEN IN EIGHT LINES ON THE CONTACT SURFACE OF THE SMOOTH AND ROUGH SHAFTS

Smooth shaft #	R_a (μm)				Average (μm)	Standard deviation (μm)
1	1.564	1.533	1.628	1.201	1.332	0.337
	1.599	1.345	1.250	0.536		
2	1.120	0.791	1.125	1.556	1.415	0.393
	1.973	1.666	1.895	1.196		
3	1.503	1.065	1.213	1.486	1.207	0.318
	1.304	1.014	1.554	0.527		
4	1.392	1.370	1.488	1.425	1.543	0.220
	1.411	1.965	1.873	1.422		
Rough shaft #	R_a (μm)				Average (μm)	Standard deviation (μm)
5	4.158	4.896	3.818	4.814	4.284	0.481
	4.556	3.344	4.346	4.341		
6	4.503	4.758	4.536	4.278	4.197	0.417
	3.545	3.553	4.305	4.098		
7	4.365	3.242	4.470	4.947	4.306	0.447
	4.404	4.316	4.428	4.274		
8	3.874	4.005	4.952	3.972	4.217	0.447
	4.352	3.537	4.229	4.814		

B. Shrink-Fit Assembly

To produce a shrink-fit assembly of the gear and shaft, the gear was placed inside a furnace for an hour to increase its inner radius to the required radius. The temperature difference necessary for the gear to obtain the required expansion over the undeformed solid shaft is given by [27]:

$$\Delta T = \frac{\delta}{\alpha\, R_{H_i}} \qquad (6)$$

where α = 12.2 x10^{-6} / ℃ for the gear material (AISI 6150 alloy steel), R_{Hi} = 14 mm, and δ = 0.025 mm. Substituting these values into Eq. (1) gives ΔT = 146 ℃, T_2 = T_1+ΔT = 25 + 146 = 171 ℃, where T_2 is the furnace temperature and T_1 is the room temperature in which the furnace is located. To avoid excessive cooling of the gear and for more suitable expansion and to get a comfortable fit, the furnace temperature was 250 ℃.

To produce a shrink-fit assembly of the gear and shaft, the gear was placed inside a furnace for an hour to increase its inner radius to the required radius. The temperature difference necessary for the gear to obtain the required expansion over the undeformed solid shaft is given by [27]:

After completing the heating process of the gear, the gear was taken out from the furnace and placed on the table, then the undeformed solid shaft was pushed and slipped inside the gear easily. After cooling, the gear contracted, and the assembly was done. This process was completed quickly in two seconds to avoid excessive cooling of the gear. Fig. 5. shows the assembled shaft and gear specimens.

The release force of specimens was tested by a universal testing machine as shown in Fig. 6. The pulling speed of this machine (testing speed) was changed from 2 to 4 mm/min for half of the specimens to achieve the DOE methodology and obtain all possible combinations.

Figure 5. Assembled shaft and gear specimens.

Figure 6. A universal tensile testing machine.

V. RESULTS AND DISCUSSION

A. Analytical and Numerical Results

The analytical solution for the release force is carried out first by using Eqs. (4) and (5) to calculate the contact pressure and the actual radius of contact between the gear and shaft, respectively, which gives R_f = 14.02 mm and P = 159.36 MPa; where R_s, v, δ, and R_{Ho} are 14.025, 0.29, 0.025, and 43 mm, respectively. Given that L = 23 mm and μ_s = 0.12, substituting the two values of the contact pressure and the actual radius of contact into Eq. (3) gives a value for the release force of F_R = 38.7 kN.

The FE model that shown in Fig. 2 is solved using COMSOL Multiphysics software to evaluate the numerical solution. Fig. 7 shows the direction of contact pressure and friction force at the contact surface where the green arrows refer to the contact pressure direction, and the pink arrows refer to the friction force direction. The contact pressure distribution is shown in Fig. 8, and it shows the irregularity of the contact pressure values at the contact surface, so the average contact pressure is calculated for all points on the contact surface, and it was 150.75 MPa. In COMSOL Multiphysics software, the release force is evaluated using integrate the contact pressure with respect to the area of the contact surface to compute the normal force then multiply this value by the statics of coefficient friction, by using the following expression $\mu_s \int P.dA$, which represents a formula for calculating the friction force between the shaft and gear. Fig. 9 shows the numerical solution of the release force

using COMSOL Multiphysics software, and it was 36.6 kN.
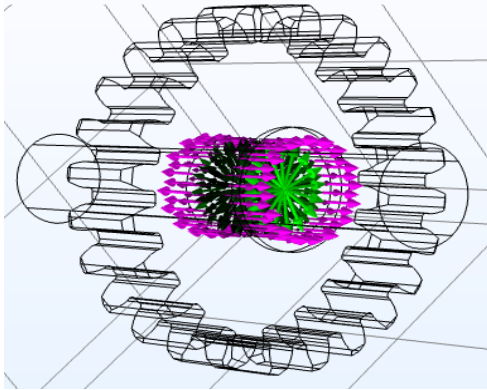
Figure 7.   Contact pressure and friction force direction.
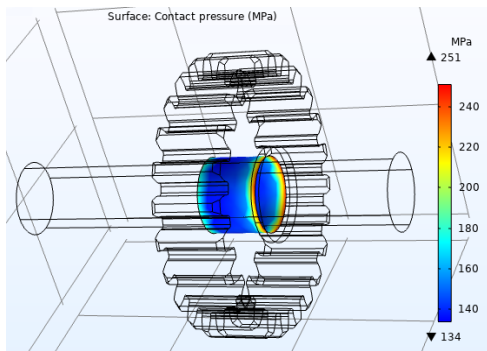
Figure 8.   Contact pressure distribution.
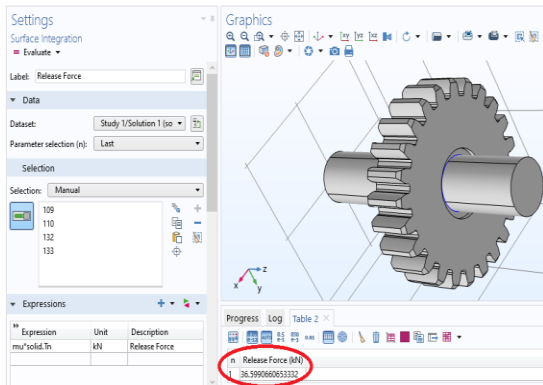
Figure 9.   Numerical solution of the release force.

B. Mesh Convergence

The mesh refinement was begun from coarse to extremely fine in COMSOL Multiphysics to observe the impact of mesh size on contact pressure and release force. Different meshes with the total number of element ranges between 7291 and 1091589 are tested to test the mesh effect on the above-mentioned quantities. It can be seen from the Table Ⅳ that for mesh number 5, all quantities will reach the stable state, i.e., the increasing of mesh refinement will lead to consumption more time by simulation process with negligible effect on accuracy. It is worth mentioning here that mesh number 5 is used for all simulations considered in this study.

TABLE IV.   DIFFERENT MESHES TO TEST THE DEPENDENCE OF CALCULATED QUANTITIES ON MESH SIZE

Mesh #	Element #	Contact pressure (MPa)	Release force (kN)
1	7291	135.21	32.82
2	12556	143.58	34.86
3	22002	142.06	34.49
4	71751	150.23	36.47
5	353156	150.75	36.60
6	1091589	150.80	36.60

C. Experimental Results

A physical assembly of the gear and shaft was produced to validate the analytical and numerical results, and it was produced under the same conditions of the analytical and numerical model such as using the same dimensions of the specimen, material used, and the static coefficient of friction. The experimental test that is shown in Fig. 10 is done by a universal testing machine on this specimen to evaluate the disassembly force which represent the experimental force required to break the gear/shaft joint. In other words, the experimental release force.

Fig. 11 shows the result of the experimental test. It can be seen from this figure that the maximum load (shown with a red circle in the figure) necessary to disassemble the gear shrink-fitted shaft joint is 35.2 kN, and this load represents the experimental release force.
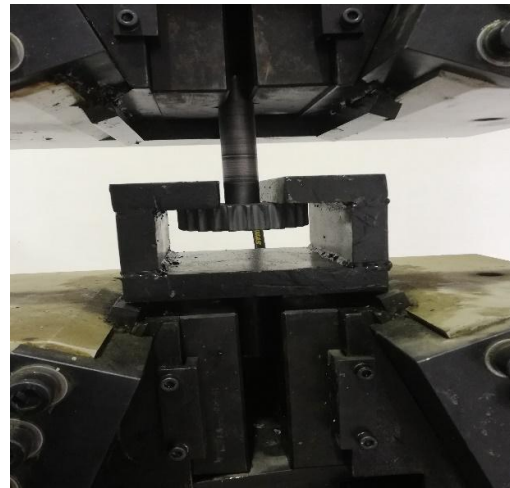
Figure 10. Experimental setup to release the gear off the shaft.
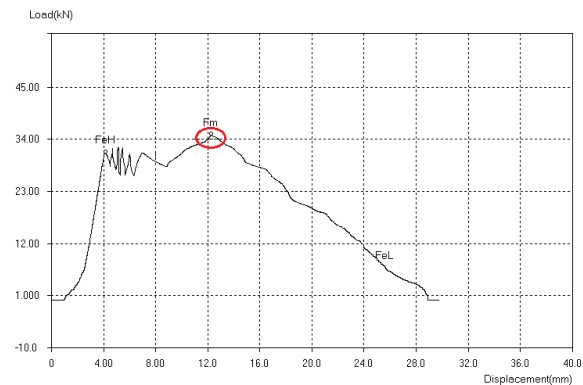
Figure 11. Disassembly force vs. axial displacement.

The comparison between the analytical, numerical, and experimental results is shown in Table Ⅴ. According to this table, the relative error of the release force between the analytical and numerical results is 5.4%, between the analytical and experimental results is 9%, and between the numerical and experimental results is 4%. The solution of the numerical model is built based on the analytical equations with some assumptions, so the error between the results can be interpreted. The relative error between the analytical and numerical results that was 5.4 % is caused by two main reasons: 1) the analytical model is a two-dimensional model, but the numerical model that used is a three-dimensional model. 2) the analytical model is built based on a cylinder fitted over a solid shaft, but the numerical model is built based on a gear (in other words a toothed cylinder) fitted over a solid shaft.

The relative error between the analytical or numerical results and the experimental results can be interpreted difficultly because the experiments represent reality and there are many factors that contribute to occur this error, so that the statistical ANOVA and DOE methodology is used to interpret this error, as presented in the next section.

TABLE V. COMPARISON BETWEEN ANALYTICAL, NUMERICAL, AND EXPERIMENTAL RESULTS

Result	Contact pressure (MPa)	Release force (kN)
Analytical results	159.36	38.7
Numerical results	150.75	36.6
Error	-	5.4%
Analytical results	159.36	38.7
Experimental results	-	35.2
Error	-	9%
Experimental results	-	35.2
Numerical results	150.75	36.6
Error	-	4%

D. Analysis of Variance

The results of the DOE-based factorial experiments are shown in Table Ⅵ. This table shows the release force as a function of the testing speed and R_a with 2 replicates. The data of the release force that are shown were run randomly using Minitab statistical software although they are shown in their standard order. The data of release force are averaged for the same levels of the factors then plotted against the different levels for each factor (R_a and testing speed) to construct the main effect plots as shown in Fig. 12. Based on these plots, it can be seen that the line of R_a factor has the maximum slope value in the plot, so the R_a is the most effective factor on the release force, and the release force increases from 35.85 to 53.5 kN (as averaged value) as R_a increases. Also, the line of testing speed factor has a small slope value in the plot, so the testing speed is not a significantly effective factor on the release force where the release force changes from 43.725 to 45.625 kN as the testing speed increases.

The interaction effect plot is constructed by plotting the release force means against the R_a for each level of the testing speed in one plot as shown in Fig. 13. This plot is used to check the interaction effect of the factors.

It can be noted from this figure that the two lines are parallel that means the changing in the release force produced from changing the levels of R_a is approximately the among the testing speed levels, so the interaction effect between R_a and testing speed is not significant.

The effect plots may not provide solid evidence on whether R_a or testing speed has a significant effect on the release force or not, especially when increasing the number of factor levels and obtaining an irregular pattern which means there are increasing and decreasing at the same pattern, thus not obtaining a clear result. So that, another statistical technique such as the analysis of variance (ANOVA) is used in the design of experiments to provide stronger and clear results.

TABLE VI. RELEASE FORCE VALUES ACCORDING TO THE 2^2-FACTORIAL DESIGN

R_a (µm)	Testing speed (mm/min)	Release force (kN) Replicates		
		1	2	Average
Smooth	2	34.2	35.8	35
Rough	2	56.8	48.1	52.45
Smooth	4	37.3	36.1	36.7
Rough	4	55.5	53.6	54.55
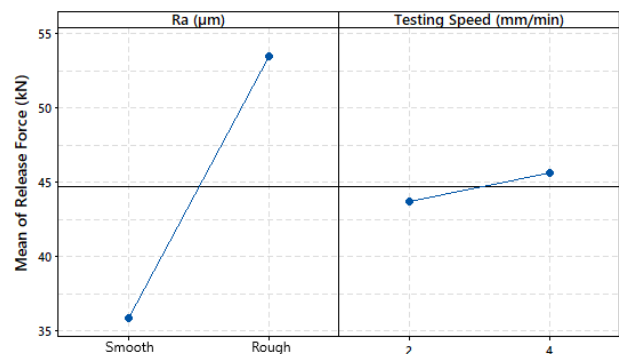
Figure 12. Main effect plots of the R_a and testing speed for means of the release force.
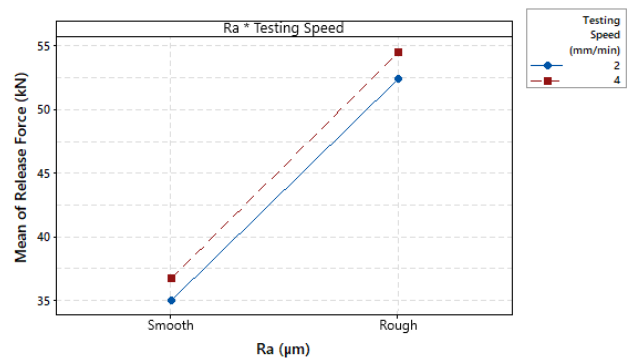
Figure 13. Interaction effect plot for means of the release force.

The analysis of variance (ANOVA) is a statistical method that is used to determine the significant factors in the experiments. This method based on a partitioning of the total variability in the response variable into

components that are consistent with a model for the experiment [28]. Thus, the first step is that assumed a suitable statistical model to explain the relationship between the response variable and the independent variables or regressor (factors). So, the following statistical model was used in this study:

$$y_{ijk} = \mu + \tau_i + \beta_j + (\tau\beta)_{ij} + \epsilon_{ijk}, \begin{cases} i = 1, 2 \\ j = 1, 2 \\ k = 1, 2 \end{cases} \quad (7)$$

Where, y_{ijk} is a random variable denoting the (ijk)th observation of the release force, μ is the grand or overall mean effect, τ_i is the effect of the ith level of the R_a, β_j is the effect of the jth level of the testing speed, $(\tau\beta)_{ij}$ is the interaction effect between the R_a and testing speed, and ϵ_{ijk} is the (ijk)th random error ~ NID $(0,\sigma^2)$ means that is normally distributed with zero mean and constant variance.

Depending on Eq. (7), the ANOVA is applied to the data in Table VI by using Minitab statistical software. The results of ANOVA are shown in Fig. 14. The P-value (in Fig. 14) is calculated and then compared to α which is called a significant level (α = 0.05 in this study). If P-value < α, this indicates that the factor has a significant effect on the response, otherwise there is no significant effect and the factor has a negligible effect. From Fig. 14, the calculated P-value for R_a, testing speed, and the interaction effect is 0.002, 0.452, and 0.934, respectively. Thus, it can be concluded that only R_a has a significant effect on the release force, and the testing speed and interaction have a negligible effect on the release force.

Also, from the same figure, there is the R^2-value which is read R-sq in the figure. This value is called the coefficient of determination, and it means the amount of variability in the data explained or accounted for by the statistical model that is presented in Eq. (7). Since the calculated R^2-value for the assumed model is equal to 93.80%, this means that 93.80% of the variability in the data in Table VI is accounted for by the model in Eq. (7), and only 6.20% of the variability in the data is credited to the error. This confirms the validity of the model in Eq. (7) and indicates that the obtained results are significant statistically.

A three-dimensional surface plot of the release force as a function of R_a and testing speed is constructed as shown in Fig. 15. This plot is useful to visualize the relationship between the release force, R_a, and testing speed, and to determine a pattern to obtain the optimal response value. It can be seen from this figure that the release force increases as R_a increases alone, and it changes slightly as testing speed increases alone because the testing speed has a negligible effect on the release force.

In addition, Fig. 16 shows a contour plot that is derived from the three-dimensional surface plot for the release force. This plot is used to search for minimums and maximums in a set of triradiate data. From this figure, it can be noted that the maximum value of the release force is obtained at the rough level of the R_a regardless of testing speed because it is a negligible effect factor. Thus,

the increased R_a alone, that means from smooth to rougher, contributes to increase the release force.

Figure 14. Mintab output for the ANOVA calculations based on the assumed statistical model in equation (7).
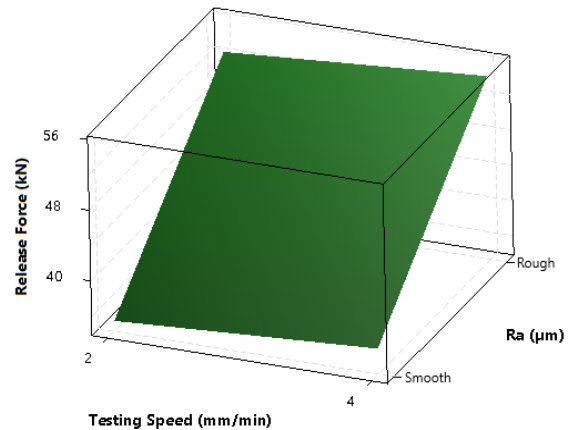
Figure 15. Three-dimensional surface plot of the release force as a function of R_a and testing speed.
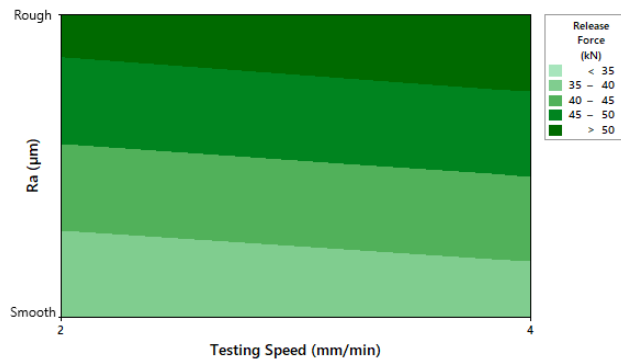
Figure 16. Two-dimensional contour plot of the release force that derived from Fig. 15.

Figure 17. Mintab output for the 95% confidence interval calculation based on the data in Table VI.

In summary of the ANOVA results, it was concluded that the testing speed and interaction between testing speed and R_a have a negligible effect on the release force, and only R_a has a significant effect on the experimental results of the release force, and this interprets the variability in the experimental results and relative error between the analytical or numerical results and the experimental results that was shown in Table Ⅴ.

Also, a 95 % confidence interval (CI) on the mean of the release force is calculated based on the data in Table Ⅵ as shown in Fig. 17. This confidence interval has a lower limit of 36.48 kN and an upper limit of 52.87 kN. The analytical result and numerical result that were respectively 38.7 kN and 36.6 kN lay within this interval, thus it can be said that the analytical result and numerical result are statistically plausible results and the difference between analytical, numerical, and experimental results that found in this study are interpreted and acceptable.

VI. CONCLUSIONS

In the scope of the results and analysis presented in this study to evaluate the release force for a gear shrink-fitted over a solid shaft, the following can be concluded:

1) The relative error between the analytical and numerical results was 5.4%, and this error is caused by two main reasons. The first is that the analytical model was a two-dimensional model, while the numerical model was a three-dimensional model. The second reason is that the analytical model was built based on a cylinder, whereas the numerical model was built based on a gear.

2) The ANOVA for the experimental results showed that testing speed and interaction between testing speed and R_a are non-significant factors in terms of their effect on the release force, and only R_a has a significant effect on the release force. Thus explains the variability in the experimental values of the release force and the relative error between the analytical or numerical results with the experimental results.

3) The analytical and numerical computations of the release force lay within the 95 % confidence interval on the mean release force established experimentally, which validates the analytical and numerical calculations and thus the underlying models developed in this study.

CONFLICT OF INTEREST

The authors declare no conflict of interest.

AUTHOR CONTRIBUTIONS

Omar Bataineh was responsible for the development of the analytical model, statistical analysis of the data, planning and supervision of this research, and correspondent author for the research paper. Ali Al-Hawari was involved in building the FE numerical model, conducting the experimental work, and producing an initial draft of the research paper.

REFERENCES

[1] R. Mott, *Machine Elements in Mechanical Design,* Pearson; 5th Edition, 2013.

[2] K. Ning, J. Wang, H. Jiang, D. Xiang, D. Hou, "Multi-objective intelligent cooperative design for the multilayer interference fit," *Mathematical Problems in Engineering,* vol. 2019, no. 1, pp. 1-15, 2019.

[3] S. Yang, Y. Ji, Y. Mo, T. Xia, "Effects of prestressing of the ring gear in interference fit on flexural fatigue strength of tooth root," *Chinese Journal of Mechanical Engineering,* vol. 32, no. 1, pp. 1-9, 2019.

[4] S. Schmid, B. Hamrock, B. Jacobson, *Fundamentals of machine elements: SI version*, CRC Press, 3rd Edition, 2014.

[5] R. Seifi and K. Abbasi, "Friction coefficient estimation in shaft/bush interference using finite element model updating," *Engineering Failure Analysis,* vol. 57, no. 1, pp. 310-322, 2015.

[6] S. Rao, *The Finite Element Method in Engineering,* Butterworth-heinemann; 5th Edition, 2017.

[7] F. Antonio, C. Luigi, D. Fazio, D. Massimo, and V. Antonio, "Enhanced aluminium foam based cylindrical sandwiches: bending behaviour and numerical modeling," *International Review on Modelling and Simulations (IREMOS),* vol. 11, no. 4, p. 198, 2018.

[8] F. Antonio and D. Massimo, "Mechanical characterization and FEM modeling of hybrid metal foam/bio-composite samples," *International Review on Modelling and Simulations (IREMOS),* vol. 10, no. 5, p. 320, 2017.

[9] B. Samya and El Boudi, "Effect of profile shift factor on contact stress and natural frequencies of spur gear," *International Review on Modelling and Simulations (IREMOS),* vol. 13, no. 6, p. 400, 2020.

[10] K. Ravi and B. Kumar, "Modal based sensitivity analysis of crack in turbine blades using validated finite element models," *International Review on Modelling and Simulations,* vol. 12, no. 5, p. 292, 2019.

[11] P. Valentino, R. Felice, S. Fabio, "Finite element modeling of superplastic forming of friction stir processed AZ31B Mg alloy," *International Review on Modelling and Simulations (IREMOS),* vol. 10, no. 6, p. 447, 2017.

[12] N. Laghzale, A. Bouzid, "Analytical modelling of elastic-plastic interference fit joints," *International Review on Modelling and Simulations (IREMOS),* vol. 9, no. 3, pp. 191–199, 2016.

[13] Z. Murčinková, P. Baron, M. Pollák, "Study of the press fit bearing-shaft joint dimensional parameters by analytical and numerical approach," *Advances in Materials Science and Engineering,* vol. 2018, no. 1, pp. 1-10, 2018.

[14] M. Yamamoto, H. Ishiduka, "Stress concentration of transition groove induced by a press-fitted part in railway axles," *International Journal of Fatigue,* vol. 97, no. 1, pp. 48-55, 2017.

[15] Y. Zhang, L. Lu, L. Zou, D. Zeng, J. Zhang, "Finite element simulation of the influence of fretting wear on fretting crack initiation in press-fitted shaft under rotating bending," *Wear,* vol. 400, no. 1, pp. 177-183, 2018.

[16] W. Song, Z. Liu, Q. Lu, "A study on effective diameter of shrink-fitted shaft-hub connection," in *Proc. 2017 International Conference on Advanced Mechatronic Systems (ICAMechS)*, Xiamen, China. IEEE, vol. 2017, no. 1, pp. 274-279, 2017.

[17] S. Chu, T. Jeong, E. Jung, "Effect of radial interference on torque capacity of press-and shrink-fit gears," *International Journal of Automotive Technology,* vol. 17, no. 5, pp. 763-768, 2016.

[18] C. Mascle, M. Balazinski, A. Mhenni, "Effect of roughness and interference on torque capacity of a shrink fitted assembly," *International Journal of Advanced Manufacturing Systems,* vol. 13, no. 1, pp. 143-158, 2011.

[19] A. Raj, A. Bhatti, P. Dhanish, "Combined effect of cylindricity, roundness and roughness on axial load-carrying ability of interference fits," in *Proc. the Institution of Mechanical Engineers, Part J: Journal of Engineering Tribology,* vol. 243, no. 11, pp. 1697-1711, 2020.

[20] R. Seifi, K. Abbasi, M. Asayesh, "Effects of contact surface roughness of interference shaft/bush joints on its characteristics," *Iranian Journal of Science and Technology, Transactions of Mechanical Engineering,* vol. 42, no. 3, pp. 279-292, 2018.

[21] O. Bataineh, "An analytical model to predict the release force in a soft hub fitted over a rigid shaft," in *Proc. the 2010 International*

Conference on Advances in Mechanical Engineering, vol. 2010, pp. 461-464, 2010.

[22] O. Bataineh and D. Dalalah, "Strategy for optimising cutting parameters in the dry turning of 6061-T6 aluminium alloy based on design of experiments and the generalised pattern search algorithm," *Int. J. Mach. Mach. Mater.*, vol. 7, no. 1–2, pp. 39–57, 2010.

[23] O. Bataineh and M. Almomani, "Applying ANOVA and DOE to study the effect of manganese on the hardness and wear rate of artificially aged Al-4.5wt%Cu alloys," *Int. J. Cast Met. Res.*, vol. 31, no. 1, 2018.

[24] O. Bataineh, "Effect of roller burnishing on the surface roughness and hardness of 6061-T6 aluminum alloy using ANOVA," *Int. J. Mech. Eng. Robot. Res.*, vol. 8, no. 4, pp. 565–569, 2019.

[25] O. Bataineh, T. Al-Hawari, H. Alshraideh, and D. Dalalah, "A sequential TPM-based scheme for improving production effectiveness presented with a case study," *J. Qual. Maint. Eng.*, vol. 25, no. 1, 2019.

[26] A. M. Hassan, O. M. Bataineh, and K. M. Abed, "The effect of time and temperature on the precipitation behavior and hardness of Al-4 wt%Cu alloy using design of experiments," *J. Mater. Process. Technol.*, vol. 204, no. 1–3, pp. 343–349, 2008.

[27] S. Schmid, B. Hamrock, B. Jacobson, *Fundamentals of Machine Elements: SI Version*, CRC Press; 3rd Edition, 2014, pp. 243-257.

[28] D. C. Montgomery, *Design and Analysis of Experiments* (New York (NY): John Wiley & Sons Inc.; 8th Edition, 2013, pp. 68-88.

Omar M. Bataineh received his B.Sc. degree from Jordan University of Science and Technology (JUST), Irbid, Jordan, in 1997, and his M.Sc. and Ph.D. degrees from the University of Minnesota (UMN), Minneapolis, MN, USA, in 2000 and 2004, respectively. He joined the Department of Industrial Engineering as an Assistant Professor at Jordan University of Science and Technology in July 2004. Then, he earned three years of leave to serve as an Assistant Professor at Prince Mohammad Bin Fahd University (PMU), Al-Khobar, Saudi Arabia, between September 2009 and August 2012. After being promoted to the rank of Associate Professor at JUST in April 2013, he spent a sabbatical year while affiliated with JUST as an Associate Professor at the American University of the Middle East (AUM) in Kuwait between January 2015 and February 2016. Currently, he continues to work at the I.E. Department of JUST.

Dr. Bataineh had consulting and training experiences provided to some international engineering firms such as Talal Abu-Ghazaleh & Co., Amman, Jordan, and Macquarie Group, Abu Dhabi, UAE. He published more than 15 articles in refereed and indexed international journals and conferences. His most recent research focuses on intelligent manufacturing, applied optimization, and lean manufacturing.
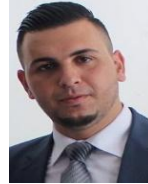
Ali H. Al-Hawari received his B.Sc. degree from Al-Balqa' Applied University (BAU), Irbid, Jordan, in 2016, and now is preparing for his M.Sc. degree from Jordan University of Science and Technology (JUST), Irbid, Jordan. The B.Sc. degree was in mechanical engineering/production and machines, and the M.Sc. degree is in industrial engineering. He worked as a teaching assistant for three semesters at Jordan University of Science and Technology in the industrial engineering department. After that, he works as an operator engineer in Korea Electric Power Corporation (KEPCO), Jordan, until today. Eng. Ali is a member of the Jordan Engineers Association (JEA).